ACCOUNTS OF CHEMICAL RESEARCH

VOLUME 9 NUMBER 7 JULY, 1976

Study of Electrogenerated Reactants Using Optically Transparent Electrodes

Theodore Kuwana*

Department of Chemistry, The Ohio State University, Columbus, Ohio 43210

William R. Heineman

Department of Chemistry, University of Cincinnati, Cincinnati, Ohio 45221

Received September 17, 1975

In 1964 the use of an optically transparent electrode (OTE) for the in situ spectral observation of an electrogenerated product by light passing through the electrode was experimentally demonstrated.[1] This idea of an OTE evolved from an earlier remark by Professor R. N. Adams to the effect, "wouldn't it be nice to have a 'see-through' electrode to spectrally identify the colored species being formed".[2] OTE's have been developed now to the point where it is relatively easy to optically examine an electrogenerated species for identification or characterization purposes. Also, the analysis of the shape of the optical absorbance as a function of time during some electrochemical perturbation can greatly assist in evaluating the mechanism and kinetics of these species.

The first OTE consisted of a glass surface which had been coated with a thin transparent film of antimony-doped tin oxide (Nesa glass). It was used for both transmission and internal reflection spectroelectrochemical experiments.[1,3] Other OTE's such as germanium plates for infrared,[4,5] thin platinum films "painted" on glass,[6] minigrids (thin wire screens),[7] and vapor-deposited metal films on transparent substrates[8-12] have been reported.

During the past 10 years, progress in OTE spectroelectrochemistry has included: (1) development and characterization of a variety of OTE and spectroelectrochemical cells; development of high sensitivity, optical monitoring systems including computer signal averaging and rapid scanning spectrophotometers; (2) computer analysis of optical absorbance (A) vs. time (t) relationships for various reaction mechanisms; (3) evaluation of kinetic rates near the diffusional limit; and (4) determination of other physiochemical information such as stoichiometry (n, number of electrons transferred), energetics ($E^{0'}$ value), molar absorptivities, and diffusion coefficients involving electrogenerated intermediates or products. Because of the experimental simplicity, most of the work has been done by transmission type spectroscopy using OTE's made from conductive thin films on transparent substrates or the minigrids.

There are also spectroelectrochemical experiments in which the light beam is reflected from the electrode surface, i.e. techniques of ellipsometry and specular reflectance. Since these techniques do not require transparency of the electrode, they will not be discussed here. Excellent discussions of these methods are available elsewhere.[13,14]

This Account, therefore, deals primarily with our experiences with spectroelectrochemistry using OTE's. It emphasizes the experimental aspects and discusses some illustrative types of reaction mechanisms amenable for study. Other sources are available for review and more detailed discussions of spectroelectrochemistry.[13-17]

Theodore Kuwana is Professor of Chemistry at The Ohio State University, Columbus, Ohio. He received his B.S. degree from Antioch College, his M.S. from Cornell University, and his Ph.D. from the University of Kansas, 1959, with Professor Ralph N. Adams. After a postdoctoral year at Caltech, he joined the staff at The University of California, Riverside. He moved to Case Western Reserve University in 1966 and to Ohio State in 1971. His major research interests are in the application of optical methods to electrochemistry, mechanistic bioelectrochemistry, and analytical instrumentation.

William R. Heineman received his B.S. degree in 1964 from Texas Tech University and his Ph.D. in 1968 with Professor Royce W. Murray at the University of North Carolina at Chapel Hill. Two years as a Research Chemist at the Hercules Research Center were followed by 2 years as a Research Associate with Professor Kuwana at Case Western Reserve University and The Ohio State University. In 1972 he joined the faculty at the University of Cincinnati where he is Associate Professor of Chemistry.

(1) T. Kuwana, R. K. Darlington, and D. W. Leedy, *Anal. Chem.*, **36**, 2023 (1964).

(2) We were studying electrooxidation of various substituted phenylenediamines where semiquinones and quinoneimines have optical absorbances in the visible region of the spectrum.

(3) W. N. Hansen, R. A. Osteryoung, and T. Kuwana, *J. Am. Chem. Soc.*, **88**, 1062 (1966); *Anal. Chem.*, **38**, 1810 (1966).

(4) H. B. Mark, Jr., and B. S. Pons, *Anal. Chem.*, **38**, 119 (1966).

(5) D. R. Tallant and D. H. Evans, *Anal. Chem.*, **41**, 835 (1969).

(6) B. S. Pons, J. S. Mattson, L. O. Winstrom, and H. B. Mark, Jr., *Anal. Chem.*, **39**, 685 (1967).

(7) R. W. Murray, W. R. Heineman, and G. W. O'Dom, *Anal. Chem.*, **39**, 1666 (1967).

(8) A. Yildiz, P. T. Kissinger, and C. N. Reilley, *Anal. Chem.*, **40**, 1018 (1968).

(9) V. S. Srinivasan and T. Kuwana, *J. Phys. Chem.*, **72**, 1144 (1968).

(10) A. Prostak, H. B. Mark, Jr., and W. N. Hansen, *J. Phys. Chem.*, **72**, 2576 (1968).

(11) T. Osa and T. Kuwana, *J. Electroanal. Chem.*, **22**, 389 (1969).

(12) W. von Benken and T. Kuwana, *Anal. Chem.*, **42**, 1114 (1970).

(13) Symp *Faraday Soc.*, **No. 4** (1970).

(14) *Adv. Electrochem. Electrochem. Eng.*, **9** (1973).

(15) N. Winograd and T. Kuwana, *Electroanal. Chem.*, **7**, (1974).

(16) T. Kuwana, *Ber. Bunsenges. Phys. Chem.*, **77**, 858 (1973).

(17) Several papers in "Intermediates in Electrochemical Reactions," *Faraday Discuss. Chem. Soc.*, **No. 56** (1973).

Table I
Optical Transmission and Electrochemical Data on Various OTE's

Type of OTE	Transmission range	Typical resistance, Ω/sq	Usable potential range, V, vs. SCE
Pt film (vapor deposited)	220–near-ir, 10–40%	15–25	See Figure 2
Hg–Pt film (electrodeposited Hg)	220–near-ir, 10–30%	10–25	+0.2 to −0.9 aqueous pH 7
Au film (vapor deposited)	220–near-ir, 10–80%	5–20	See Figure 2
Sb-doped tin oxide (Nesa)	360–near-ir on glass, 70–85%	5–20	+1.2 to − 0.6 aqueous pH 7
	240–near-ir on quartz, 50–85%	Same	
Sn-doped indium oxide (Nesatron)	Same as tin oxide	5–20	Same as tin oxide
Carbon film electrode	Ir (4–15%, IRS[a])	2000–5000	+0.5 to −1.4 aqueous sodium borate
Ge	Ir (4–30%, IRS)	2000–5000	−0.3 to −1.3 aqueous sodium borate
Au minigrid	Uv–visible-ir, 22–80%	<0.1	Same as Au film
Hg–Ni minigrid	Uv–visible-ir, 22–80%	<0.1	+0.2 to −1.0 aqueous pH 7
Hg–Au minigrid	Uv–visible-ir 22–80%	<0.1	+0.2 to −1.4 aqueous pH 7

[a] IRS, internal reflectance spectroscopy.

Types of Optically Transparent Electrodes

Table I summarizes the types of OTE and their optical and electrochemical characteristics. Most of the OTE's are prepared by depositing a thin film of metal such as Pt or Au[8–12] or a "doped" oxide such as a tin oxide (Nesa)[1,3,18] or indium oxide (Nesatron)[18] on a transparent substrate (glass or quartz). Optical transparency is due to the thinness of the conducting film, and a compromise is made between the resistance (8–20 Ω/sq) and the transmission (60–95%). A mercury-surfaced OTE has also been prepared by electrochemically depositing a thin film of mercury on a Pt film.[19] Germanium[4,5] and carbon film surfaces[20] have been used in the infrared region.

An interesting variation of the OTE is the minigrid electrode which consists of a wire mesh of 40 to 800 wires/cm.[7] The light is transmitted through the microscopic holes between the wires. Although the minigrid is a wire mesh, it functions essentially as a planar electrode after electrolysis has proceeded for sufficient time that the diffusion layer depth becomes large compared to the wire and hole dimensions (11, 88, and 385 ms for minigrids of 800, 400, and 200 wires/cm, respectively).[21] The gold minigrid has been particularly useful in the construction of optically transparent thin layer cells.

The choice of which OTE to use is not always clear. The main considerations are, of course, the optical and potential regions of interest. Also, the resistance of the OTE must be sufficiently low to enable the electrode potential to be controlled. As may be seen from Table I, the available OTE's provide a reasonably wide optical window extending from the ultraviolet into the infrared. A moderately wide working range of potential is also attainable, particularly in nonaqueous media.[11]

Representative background spectra and current–potential (i–E) curves of the thin metal films (Au and Pt) and doped oxides (SnO_2 and In_2O_3) are reproduced in Figures 1 and 2. The spectrum of an Au minigrid is also shown in Figure 1 for comparison. Pt on glass or quartz acts as a neutral density filter, and the percent transmission depends on the film thickness. Au has an excellent optical window with a maximum transmission

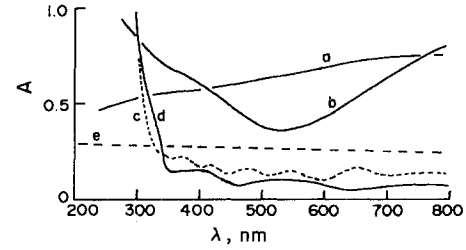

Figure 1. Transmission spectra of OTE: (a) Pt on quartz, 11 Ω/sq; (b) Au–bismuth oxide on quartz, 2.5 Ω/sq; (c) SnO_2 on quartz, 6–8 Ω/sq; (d) In_2O_3 on quartz, 10 Ω/sq; (e) Au minigrid, 200 wires/cm.

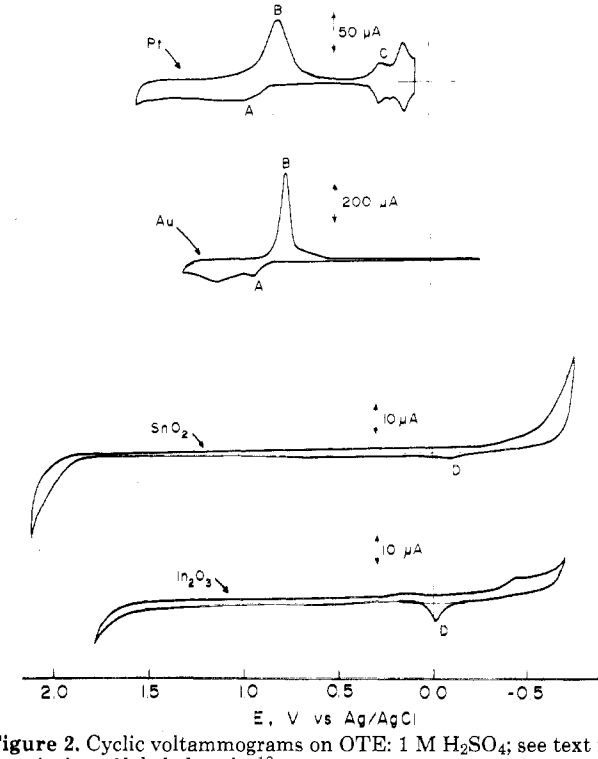

Figure 2. Cyclic voltammograms on OTE: 1 M H_2SO_4; see text for description of labeled peaks.[18]

in the visible at ca. 540 nm. Both SnO_2 and In_2O_3 transmit greater than 80% in the visible, with interference waves often present on the background spectra depending on film thicknesses. The transmittance at shorter wavelengths is limited by the optical characteristics of the substrate material and the valence to conductance band absorption of the semiconductor. The long-wavelength cutoff in the near infrared can be approximated from the free electron population and usually occurs between 1 and 2 μm. The minigrid transmittance varies from 22 to 82%, depending upon

(18) N. R. Armstrong, A. W-C. Lin, M. Fujihira, and T. Kuwana, *Anal. Chem.*, **48**, 741 (1976).
(19) W. R. Heineman and T. Kuwana, *Anal. Chem.*, **43**, 1075 (1971); **44**, 1972 (1972).
(20) J. S. Mattson and C. A. Smith, *Anal. Chem.*, **47**, 1122 (1975).
(21) M. Petek, T. E. Neal, and R. W. Murray, *Anal. Chem.*, **43**, 1069 (1971).

the number of wires per centimeter. Since light passes through holes in the minigrid, the optical window is essentially unlimited.[22]

The *i–E* curves in Figure 2 show current waves corresponding to electrode surface or solvent redox reactions which occur as the potential applied to the electrode is scanned. Ideally, one would like a wide potential range between solvent oxidation and reduction with no intermediate redox reactions (current waves). In Figure 2, the *i–E* peaks labeled A and B on the Pt and Au OTE's correspond to surface oxidation of the metal film to the oxide state and subsequent reduction. Such peaks are not pronounced for SnO_2 and In_2O_3 since these surfaces are already oxidized. Thus, it appears at first glance that a much wider potential region is available on the oxide electrodes than on Pt or Au. However, caution must be exercised in the usage of these oxide OTE's *at very positive potentials* where the faradaic current may become independent of the electroactive species and become limited mainly by the internal charge transport process of the semiconductor.[23]

Peak C for the Pt film corresponds to the well-known hydrogen adsorption region. This region occurs near the reversible potential for hydrogen on Pt and limits the useful cathodic potential range. The cathodic limit is moved ca. 400 mV negative for the Hg–Pt OTE. Both Pt and Au films are quite unforgiving if the potential moves into the hydrogen generation region, causing the films to be rapidly and irreversibly removed. The hydrogen overpotential on SnO_2 and In_2O_3 electrodes is fairly large.

Small waves (labeled D) are observed as the potential moves anodically, supposedly due to some finite oxide formation. At potentials of hydrogen generation, the surface appears to be reduced to the metallic state.

The gold minigrid behaves similarly to the Au film OTE. The negative potential limit of minigrids can be extended by ca. 400 mV by depositing a thin mercury film on a gold[24] or nickel minigrid.[25]

There is need for further improvements in OTE's, particularly with respect to the surface conductivity and the optical transmission in the shorter uv and the infrared regions of the spectrum. The minigrid electrode is quite advantageous for these spectral regions and also has a very low resistance.

Spectrocoulometry

The small volume, OTE sandwich-type cell (Figure 3) has been extremely convenient for the determination of the spectral features of electrogenerated species. For example, spectra are shown in Figure 4 for the generation of 1,1′-bibenzyl-4,4′-bipyridylium radical cation (commonly called benzyl viologen, $BV^{\cdot+}$) at a tin oxide OTE:

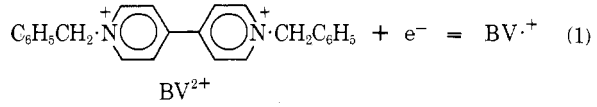

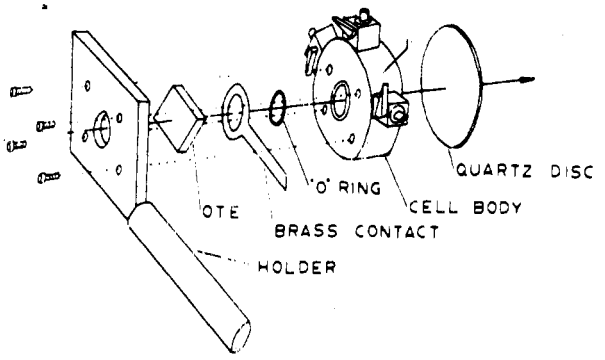

Figure 3. Spectroelectrochemical transmission cell. Sandwich cell assembly. Valves for connection with degassing bulb and reference and auxiliary electrodes.[27]

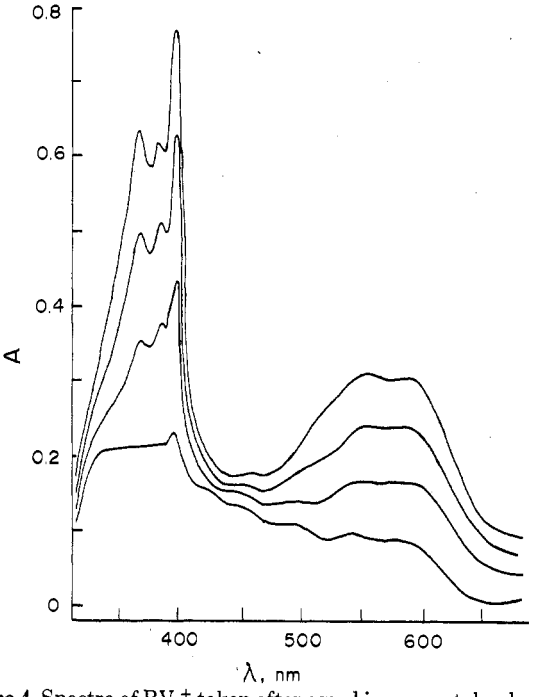

Figure 4. Spectra of $BV^{\cdot+}$ taken after equal incremental reductions of BV^{2+} at SnO_2 OTE. Sandwich cell.[26]

The absorbance maxima at wavelengths of 372, 400, 555, and 595 nm were linearly proportional to the electrochemical charge, which enabled molar absorptivities to be calculated.[26] The radical cation was found to be stable in aqueous pH 7 buffer when O_2 was rigorously excluded. Most spectroelectrochemical studies are initiated with this simple experiment.

Another area in which spectrocoulometry has been very useful to us has been in the determination of spectral properties, stoichiometry, and energetics of heme proteins such as cytochrome *c* and cytochrome *c* oxidase. Since heterogeneous electron transfer from the electrode to these hemes is extremely slow, redox titrations have been performed by the coulometric generation of mediator titrants[27–30] which were selected for reduction or oxidation depending on their redox potentials (e.g., benzyl viologen radical cation electrogenated for reduction; ferricyanide, or 1,1-bis(hydroxy-

(22) W. R. Heineman, J. N. Burnett, and R. W. Murray, *Anal. Chem.*, **40**, 1974 (1968).
(23) R. Memming and F. Mollers, *Ber. Bunsenges. Phys. Chem.*, **76**, 470 (1972); **76**, 476 (1972); **76**, 610 (1972).
(24) M. L. Meyer, T. P. DeAngelis, and W. R. Heineman, *Anal. Chem.*, submitted for publication.
(25) W. R. Heineman, T. P. DeAngelis, and J. F. Goelz, *Anal. Chem.*, **47**, 1364 (1975).
(26) E. Steckhan and T. Kuwana, *Ber. Bunsenges. Phys. Chem.*, **78**, 253 (1974).
(27) F. M. Hawkridge and T. Kuwana, *Anal. Chem.*, **45**, 1021 (1973).
(28) W. R. Heineman, T. Kuwana, and C. R. Hartzell, *Biochem. Biophys. Res. Commun.*, **49**, 1 (1972); **50**, 892 (1973).
(29) T. Kuwana and W. R. Heineman, *Bioelectrochem. Bioenerget.*, **1**, 389 (1974).
(30) L. N. Mackey, T. Kuwana, and C. R. Hartzell, *FEBS Lett.*, 326 (1973).

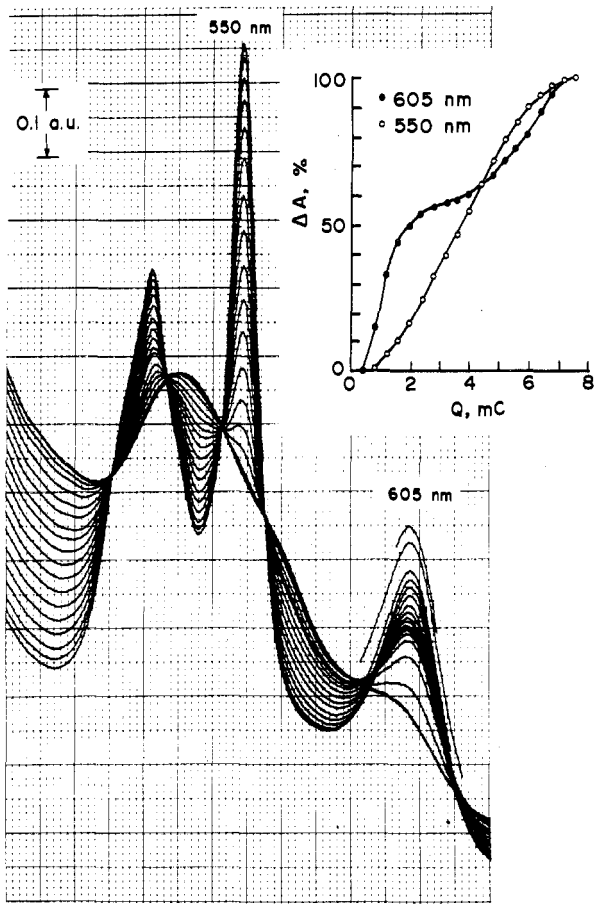

Figure 5. Spectrocoulometric titration of cytochrome *c* (17.5 μM) and cytochrome *c* oxidase (6.3 μM) by reduction with $MV^{\cdot+}$ generated at SnO_2 OTE. Each spectrum recorded after generation of 5×10^{-9} equiv (0.5 mC) of $MV^{\cdot+}$.[28]

methyl)ferricinium electrogenerated for oxidation). Thus, the potential applied to the OTE determined whether reductant or oxidant was generated.

Figure 5 illustrates typical spectra obtained for the reduction of a mixture of cytochrome *c* and cytochrome *c* oxidase initially in the fully oxidized state.[28] Each spectrum was recorded after the coulometric addition of 5.0 nequiv of reductant, the methyl viologen radical cation ($MV^{\cdot+}$). The reaction sequence is an EC catalytic regeneration (mechanism 3, Table II):

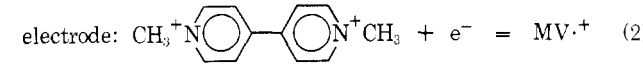

solution: $MV^{\cdot+}$ + cyto *c* (ox)

$$\underset{k_{-3}}{\overset{k_3}{\rightleftharpoons}} MV^{2+} + \text{cyto } c \text{ (red.)} \quad (3)$$

The absorbance increase at 605 nm corresponds to the reduction of the two heme components of cytochrome *c* oxidase; the increase at 550 nm corresponds to the reduction of the heme in cytochrome *c*. Evaluation of the relative shapes of the absorbance at these two wavelengths as a function of coulometric charge (see inset of Figure 5) indicated the sequence of the titration: one heme of oxidase was reduced initially followed by the heme of cytochrome *c*, and then finally the low potential heme of oxidase. The total amount of charge required for complete reduction of the mixture corresponded to an *n* value of 5 (one electron for cytochrome *c* and four electrons for the two hemes and the two copper centers in oxidase). Comparison between the experimental *A–Q* curves and computer-simulated curves for various $E^{0\prime}$ values (assigned to each redox component of the oxidase relative to a known $E^{0\prime}$ value for cytochrome *c*)[30] has provided evaluation of $E^{0\prime}$ values.

An important feature of this *A–Q* approach is the ability to evaluate $E^{0\prime}$ values of nonabsorbing components (e.g., the coppers in oxidase) in comparison to potentiometric or log–log absorbance methods.[28,30] Another advantage of the coulometric method is the convenience of repetitively cycling between oxidized and reduced states in the presence of an oxidizing and reducing mediator. Cycling allows the study of reversibility and time dependent effects.

The ultimate in small volume cells (30–50 μl) is the so-called OTTLE (optically transparent thin layer electrode) cell.[7] It is constructed in a "thin-layer" configuration by sandwiching, for example, an Au minigrid between two microscope slides which are separated by 0.05 to 0.3 mm with Teflon tape spacers. Complete electrolysis of electroactive materials in the thin layer can be achieved in seconds with diffusion as the sole mode of mass transport. Its major use has been in the coulometric determination of *n* values with simultaneous acquisition of spectral data. Reported examples are: the study of acetylacetonate ligand exchange reactions for iron(II)–iron(III) in acetonitrile;[31] the reduction of ninhydrin in acetonitrile (infrared);[22] the oxidation of rubrene in benzene–acetonitrile;[8] the reduction of 1-hydroxy-9,10-anthraquinone, 1,8-dihydroxy-9,10-anthraquinone, and 9,10-anthraquinone[32,33] in nonaqueous solvents; the reduction of acetylacetone in acetonitrile;[34] the reduction of substituted porphyrins in aprotic[35] and aqueous[36] media; the reduction of the mixed valence μ-pyrazine-decaaminediruthenium(II,III) complex;[37] and reduction of vitamin B_{12} in a mercury-nickel OTTLE.[38]

Because the transport time of any species across the width of the thin layer solution is short, the establishment of redox *equilibrium* between electrode and solution is relatively rapid. This unique property of the OTTLE cell has been applied to the measurement of $E^{0\prime}$ and *n* values of cytochrome *c*.[39,40] The concentration ratio of oxidized to reduced cytochrome *c* was controlled by the electrode potential with 2,6-dichlorophenolindophenol serving as an electron-transfer mediator. For a series of applied potentials, the concentration ratio of redox states was determined from the optical absorbance at 550 nm. The $E^{0\prime}$ and *n* values were calculated from the usual Nernstian plot. The results are illustrative of the excellent precision of the method: $n = 1.00 \pm 0.01$ and $E^{0\prime} = 262 \pm 1$ mV (results for five samples)

Recently, Ke and Hawkridge[41] have configured the

(31) W. R. Heineman, J. N. Burnett, and R. W. Murray, *Anal. Chem.*, **40**, 1970 (1968).
(32) I. Piljac and R. W. Murray, *J. Electrochem. Soc.*, **118**, 1758 (1971).
(33) M. Wightman and R. W. Murray, private communication.
(34) T. E. Neal and R. W. Murray, *Anal. Chem.*, **42**, 1654 (1970).
(35) G. Peychal-Heiling and G. S. Wilson, *Anal. Chem.*, **43**, 545, 550 (1971).
(36) B. P. Neri and G. S. Wilson, *Anal. Chem.*, **44**, 1002 (1972); **45**, 442 (1973).
(37) V. S. Srinivasan and F. C. Anson, *J. Electrochem. Soc.*, **120**, 1359 (1973).
(38) T. M. Kenyhercz, T. P. DeAngelis, B. J. Norris, W. R. Heineman, and H. B. Mark, Jr., *J. Am. Chem. Soc.*, **98**, 2469 (1976).
(39) W. R. Heineman, B. J. Norris, and J. F. Goelz, *Anal. Chem.*, **47**, 79 (1975).
(40) B. J. Norris, M. L. Meckstroth, and W. R. Heineman, *Anal. Chem.*, **48**, 630 (1976).

Table II
Electrode Mechanisms Studied by Spectroelectrochemistry

Mechanism	Reaction designation	Generalized reaction schemes	Example systems[a]	References
1. Electron transfer	E	$A = A^+ + e^-$	$MV^{2+} + e^- \rightleftharpoons MV^{\cdot+}$	15, 43
2. Following chemical reaction (EC mechanism)	E	$A = A^+ + e^-$		15, 55, 62
	C	$A^+ + Z \xrightarrow{k} P$		
3. Catalytic regeneration	E	$A = A^+ + e^-$	$Fe(CN)_6^{4-} \rightleftharpoons Fe(CN)_6^{3-} + e^-$	15, 43, 44, 55, 64
	C	$A^+ + Z \xrightarrow{k} A + Z^+$	$Fe(CN)_6^{3-} + AH_2 \rightleftharpoons Fe(CN)_6^{4-} + A + 2H^+$	
4. ECE mechanism	E	$A = A^+ + e^-$		15, 52
	C	$A^+ + Z \xrightarrow{k} AZ^+$		
	E	$AZ^+ \rightarrow AZ^{2+} + e^-$		
5. Reproportionation	E	$A = A^{2+} + 2e^-$	$Ta_6Br_{12}^{2+} \rightleftharpoons Ta_6Br_{12}^{4+} + 2e^-$	15, 51
	C	$A + A^{2+} \underset{k_{-1}}{\overset{k_1}{\rightleftarrows}} 2A^+$	$Ta_6Br_{12}^{2+} + Ta_6Br_{12}^{4+} \rightleftharpoons 2Ta_6Br_{12}^{3+}$	
	E	$A^+ = A^{2+} + e^-$	$Ta_6Br_{12}^{3+} \rightleftharpoons Ta_6Br_{12}^{4+} + e^-$	
6. Reproportionation with electrophilic addition	E	$A + 2e^- = A^{2-}$		52, 63
	C	$A + A^{2-} \underset{k_{-1}}{\overset{k_1}{\rightleftarrows}} 2A^-$		
	E	$A^- + e^- = A^{2-}$		
	C	$A^{2-} + Z \xrightarrow{k_2} A^{2-}$		
7. Disproportionation and nucleophilic addition	E	$A = A^+ + e^-$		52, 53, 55
	C	$2A^+ \rightleftarrows A^{2+} + A$		
	C	$A^{2+} + Z \rightarrow AZ^{2+}$		
8. Half Regeneration	E	$A = A^+ + e^-$	$DPA \rightleftarrows DPA^+ + e^-$	52, 53, 65
	C	$A^+ + Z \rightarrow AZ^+$	$DPA^{\cdot+} + H_2O \rightarrow DPA(OH)\cdot + H^+$	
	C	$AZ^+ + A^+ \rightarrow AZ^{2+} + A$	$DPA\cdot + DPA^{\cdot+} \rightarrow DPA(OH)^+ + DPA$	
9. Cross-HETR	E	$A = A^+ + e^-$	$TAA \rightleftharpoons TAA^{\cdot+} + e^-$	15, 51
	E	$Z = Z^+ + e^-$	Ferrocene $\rightleftharpoons$ ferricinium $+ e^-$	
	C	$A + A^+ \underset{k_{-1}}{\overset{k_1}{\rightleftarrows}} Z^+ + Z$	TAA + ferricinium $\rightleftharpoons TAA^{\cdot+}$ + ferrocene	
10. Preceding chemical reaction	C	$AB \rightleftarrows A + B$		55
	E	$A = A^+ + e^-$		
11. EEC Mechanism	E	$A + e^- = A^-$	$py + e^- \rightleftharpoons py^-$	63
	E	$A^- + e^- = A^{2-}$	$py^- + e^- \rightleftharpoons py^{2-}$	
	C	$A^{2-} + Z \rightarrow$ product	$py^{2-} + HR \rightarrow pyH^- + R^-$	

[a] MV^{2+}, 1,1′-dimethyl-4,4′-bipyridilium dication (methyl viologen or paraquat); AH_2, ascorbic acid; DPA, 9,10-diphenylanthracene; TAA, tri-*p*-anisylamine; py, pyrene.

OTTLE in a quartz cell which allows them to study redox equilibria, optical spectra, flash photolysis, fluorescence emission, and circular dichrosim of photosynthetic reaction center particles (photosystems I and II). Their work nicely illustrates the versatility and convenience of OTTLE cells. We believe that these cells will see much greater use in the future, particularly in the study of biocomponents where the small volume will be advantageous for working with scarce materials.

Reaction Mechanisms and Kinetics

Mechanisms of electrode reactions and rate constants of coupled homogeneous chemical reactions can be determined by detailed analysis of the shape of the absorbance response as a function of time (A–t curve) during the electrochemical generation of a reactive species under carefully controlled conditions. Representative electrochemical mechanisms where the A–t behaviors have been analyzed are listed in Table II. References in the last column of the table should be consulted for experimental details and the manner of analyzing actual A–t curves for mechanistic and kinetic information.

For *initial* diagnosis of a possible mechanism for an electrode process, cyclic voltammetry and spectrocoulometry have been the preferred experimental methods. These methods provide information for the selection of the appropriate potential to generate reactants (e.g., A^+; see Table II for mechanisms) and the optimum wave-

(41) B. Ke and F. M. Hawkridge, unpublished results.

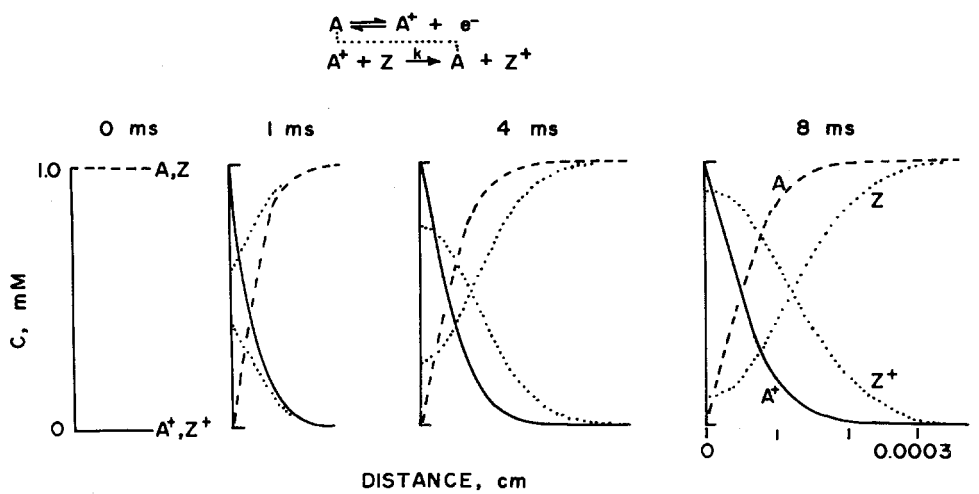

Figure 6. Concentration–distance profiles claculated for EC catalytic regeneration mechanism at t = 0, 1 ms, 4 ms, and 8 ms during potential step (chromoamperometric) experiment. $k = 10^7$ M^{-1} s^{-1}. Initial concentrations: [A] = [Z] = 10^{-3} M, [A±] = [Z±] = 0. Diffusion coefficients = 10^{-6} cm^2 s^{-1}.[29]

length for optical monitoring. If A^+ is short-lived, its spectrum can be obtained by a point-by-point wavelength monitoring during successive electrogenerations or by the use of a rapid scanning spectrometer (RSS).

Bewick and co-workers have mapped the spectrum of thianthrene radical cation using a point-by-point reflection method.[42] The use of a RSS instrument is much more convenient. Commercial units are now available with scan times in the order of 1 ms per spectrum and with wavelength ranges extending from the uv to the near-ir. The main problem of spectral acquisition at short times is how to generate sufficient quantities of the short-lived species to obtain a well-defined spectrum. Signal-averaging techniques are exceedingly useful, and by synchronizing the potentiostat with a RSS, the electrochemical experiment can be repeated several hundred times and the spectrum averaged. Using computer control on-line with signal averaging, we have recently been able to acquire spectra of species with half-lives the order of 1 ms.

The electrochemical method of choice has been chronoamperometry for quantitative A–t experiments. In this method, the potential of the OTE is stepped to a value such that reactant is generated at a diffusion-controlled rate. When a stable product is generated (reaction 1, Table II) and optically monitored during the chronoamperometric experiment, the resulting absorbance, A, increases linearly with the square root of time, $t^{1/2}$, as described by the relationship:

$$A = \frac{2C^0\epsilon D^{1/2}t^{1/2}}{\pi^{1/2}} \qquad (4)$$

where C^0 is the bulk concentration of the electroactive species, ϵ is the molar absorptivity of the optically monitored product, and D is the diffusion coefficient of the electroactive species. For other mechanisms listed in Table II, the shape of the A–t curve will deviate from that given by equation 4.

Using the EC catalytic regeneration again as an example (see mechanism 3, Table II) let us examine the c–x–t (concentration–distance–time) profiles and A–t curves. In Figure 6, the c–x–t profiles are computer calculated for the case where the concentration of initial reactants, A and Z, are equal and the product concentrations are zero, and where the rate constant of the chemical reaction is 10^7 M^{-1} s^{-1}. If the light beam is *only* monitoring the product of the E step of the EC mechanism at some set wavelength, the shape of the A–t curves for various rate constants appear as those shown in Figure 7A.

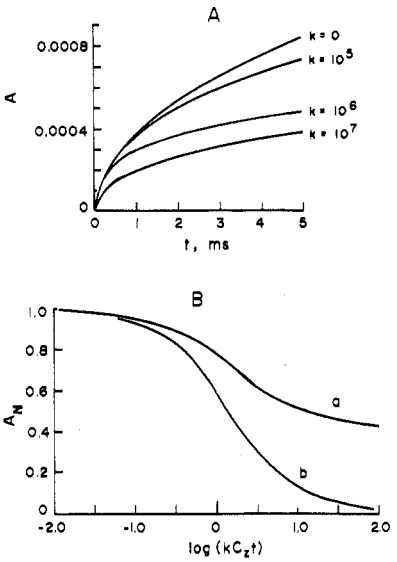

Figure 7. (A) Transmission A–t curves calculated for EC catalytic regeneration mechanism during potential step (chronoamperometric) experiment. Species A^+ optically monitored. k = 0, 10^5, 10^6, 10^7 M^{-1} s^{-1}. $\epsilon_{A^+} = 10^4$ M^{-1} cm^{-1}. See Figure 6 for other conditions.[29] (B) Normalized absorbance working curves for EC mechanisms. (a) Mechanism 3, Table II, A^+ optically monitored. (b) Mechanism 2, Table II, A^+ optically monitored.

Experimentally, A–t curves are obtained in the presence (A_k) and absence ($A_{k=0}$) of reactant Z. A value of k is then determined by fitting values of normalized absorbance, A_N ($A_N = A_k/A_{k=0}$), to a computer-calculated working curve of A_N as a function of the dimensionless parameter, log (kC_Zt). Curve a of Figure 7B is an example. Use of A_N is convenient since it becomes unnecessary to know values of ϵ and D for the reactants. For comparison purposes, curve b of Figure 7B is for a nonregenerative EC mechanism (reaction 2, Table II). Experimental verification of the EC catalytic mechanism has been from the electrooxidation of ferrocyanide to ferricyanide in the presence of ascorbic acid (aqueous, SnO_2 OTE),[43,44] the electrooxidation of tri-*p*-anisylamine in the presence of cyanide ion (acetoni-

(42) A. W. B. Aylmer-Kelly, A. Bewick, P. R. Cantrill, and A. M. Tuxford, *Faraday Discuss. Chem. Soc.*, **No. 56**, 96 (1973).

trile, Pt OTE),[44] the reduction of Ti(IV) in the presence of hydroxylamine (aqueous, Au minigrid),[45] and the reduction of MV^{2+} in the presence of cytochrome *c* (aqueous, SnO_2 OTE).[46]

The methyl viologen–cytochrome *c* reaction is worth examining in some detail to illustrate experimental complications. Since $E^{0\prime}$ of cytochrome *c* is 258 mV vs. NHE compared to the negative value of −358 mV for methyl viologen, the K_{eq} of reaction 3 is very large, and, although cytochrome *c* should be reduced more easily at the electrode than $MV^{\cdot+}$, the overpotential for *c* is sufficiently large that reduction of cytochrome *c* proceeds quantitatively through reactions 2 and 3. Earlier results[26] using signal-averaged, step-relaxation times of 1:100 and monitoring at a wavelength of 605 nm for $MV^{\cdot+}$ gave rates considerably less than those obtained by pulse radiolysis.[47]

Reevaluation by simulation of *c–x–t* and *A–t* curves for various experimental parameters revealed that (1) the absorbance contribution at 605 by cytochrome *c* was not negligible, and (2) the smaller *D* value of cytochrome *c* compared to viologen resulted in gradual depletion of cytochrome *c* from the diffusion-reaction layer during the step-relaxation (1:100 time ratio) experiment. With absorbance correction and step-relaxation times the order of 10 000 to 20 000, a lower limit of 10^8 M^{-1} s^{-1} could be assigned to a value of k_3 which is closer to the pulse radiolysis value of 2.1×10^8 M^{-1} s^{-1}.[47] Ryan and Wilson[48] have also discussed similar spectroelectrochemical problems and corrections.

For determining kinetic rates of chemical reactions which involve electrogenerated reactants, spectroelectrochemistry offers the widest kinetic range presently available with electrochemical techniques. With absorbance sensitivities of 10^{-5} to 10^{-6} au through signal averaging and with time resolutions of 5–10 μs (these are state of the art values),[49,50] it is possible to evaluate bimolecular kinetic rates near the diffusional limit (10^8–10^9 M^{-1} s^{-1}). For example, rate constants of 3×10^9 M^{-1} s^{-1} for the reproportionation (reaction 5, Table II) of methyl viologen[51] and 1.5×10^9 M^{-1} s^{-1} for the heterogeneous electron exchange (reaction 9, Table II) between tri-*p*-anisylamine and diacetylferricinium ion[51] have been measured by coupling internal reflection spectroscopy with signal averaging. Using a moderately fast potentiostat, one can rather easily step the potential and establish potential control of the electrode within 0.1 to 1 ms. At these times, bimolecular rates of 10^5 to 10^6 M^{-1} s^{-1} are determinable. These rates are competitive with most of the transient electrochemical methods for determining kinetic rates of chemical follow-up reactions.

Spectroelectrochemistry has been quite successfully applied to verify suspected mechanisms of electrode reactions. The *A–t* curve can be computer simulated for the suspected mechanism and then matched against the experimental one. (Figure 7B illustrates differences in working curves for two mechanisms.) An excellent example of this approach has been the elucidation of the electrochemical mechanism(s) for the nucleophilic addition of pyridine, hydroxyl, cyanide, or water to cation radicals derived from aromatic hydrocarbons and heterocyclic fused rings such as 9,10-diphenylanthracene (DPA), thianthrene, phenoxine, phenazine, etc. Three different reaction mechanisms which have been proposed (ref 52 and references therein) are: (1) the ECE mechanism, (2) disproportionation with nucleophilic addition, and (3) half-regeneration. As the reaction sequences in Table II show, the dication is the species undergoing nucleophilic addition in the disproportionation mechanism whereas the radical cation is the reactive species in ECE and half-regeneration mechanisms. These mechanisms also involve a homogeneous electron-transfer reaction. In all cases the final product of the fast reaction is AZ^{2+} which may then undergo further slow reactions.

Using DPA as a test case, Blount and co-workers[53,54] examined the *A–t* curves using several nucleophiles (e.g., H_2O, pyridine, H_2S, etc.). The rate law and kinetics best fit a reaction which proceeded through the *radical cation* and ruled out *radical ion disproportionation* in or before the rate-determining step. Thus, the half-regeneration (reaction 8, Table II) mechanism appeared to rationalize the experimental A_N–*t* data. DPA in the presence of chloride or bromide ion gave electron-transfer products rather than those expected from nucleophilic addition. How general the half-regeneration mechanism is for the other cation radicals with various nucleophiles remains to be demonstrated.

As suggested, the *A–t* curves can provide diagnostics of mechanism. The experimental and calculated curves must match closely over a time range of a factor of 50 or more. Also, the computer simulation of *c–x–t* and *A–t* for several possible mechanisms should be made for comparison purposes. Assessment of the "correctness" of these simulations is not always easy to make. If possible, results from potential step, double potential step, and step-relaxation methods should be analyzed and should be in agreement. Li and Wilson[55] have correlated very nicely the diagnostic criteria for several mechanisms, including consideration of overlapping optical bands. Generalized computer programs for digital simulations are available.[55,56]

Conclusion

We believe that spectroelectrochemistry using OTE's will continue to grow with new developments and application areas. Improvements in OTE's will be forthcoming in terms of conductivity, transmittance, and surface stability, particularly for use in the infrared and uv. New optical techniques such as resonance Raman spectroscopy[57] appear promising for enhanced molec-

(43) N. Winograd, H. N. Blount, and T. Kuwana, *J. Phys. Chem.*, **73**, 3456 (1969).
(44) H. N. Blount, N. Winograd, and T. Kuwana, *J. Phys. Chem.*, **74**, 3231 (1970).
(45) M. Petek, T. E. Neal, R. L. McNeely, and R. W. Murray, *Anal. Chem.*, **45**, 32 (1973).
(46) L. Mackey, E. Steckhan, and T. Kuwana, *Ber. Bunsenges. Phys. Chem.*, **79**, 587 (1975).
(47) E. J. Land and A. J. Swallow, *Ber. Bunsenges. Phys. Chem.*, **79**, 436 (1975).
(48) M. D. Ryan and G. S. Wilson, *Anal. Chem.*, **47**, 885 (1975).
(49) J. E. Davis and N. Winograd, *Anal. Chem.*, **44**, 2152 (1972).
(50) N. Winograd and T. Kuwana, *Anal. Chem.*, **43**, 252 (1971).
(51) N. Winograd and T. Kuwana, *J. Am. Chem. Soc.*, **92**, 224 (1970); **93**, 4343 (1971).
(52) R. F. Broman, W. R. Heineman, and T. Kuwana, *Faraday Discuss. Chem. Soc.*, **No. 56**, 16 (1973).
(53) H. Blount, *J. Electroanal. Chem.*, **42**, 271 (1973).
(54) D. T. Shang and H. N. Blount, *J. Electroanal. Chem.*, **54**, 305 (1974); J. F. Evans and H. N. Blount, private communication.
(55) C. Li and G. S. Wilson, *Anal. Chem.*, **45**, 2370 (1973).
(56) N. Winograd (Purdue University), H. Blount (University of Delaware), G. Wilson (University of Arizona), and our groups have available similar digital simulation programs.

ular specificity and sensitivity. Although not discussed here, it is possible to probe phenomena associated with the interphase of the electrode surface. Examples are the evaluation of optical constants of the electrode surface,[58,59] the observation of surface adsorption of anions and Pb^{2+} complexes on a Hg–Pt OTE,[19] the study of organic adsorption by internal reflection spectroscopy,[60,61] and protein adsorption on Ge OTE by infrared internal reflection spectroscopy.[20] The main utility of OTE will undoubtedly be to assist in the elucidation of electrode mechanisms and the evaluation of associated kinetics of homogeneous reactions. We hope that chemists with interests in organic, inorganic, and biochemical redox systems will be encouraged to use spectroelectrochemistry. Perhaps this Account will stimulate them to try.

(57) D. L. Jeanmaire, M. R. Suchanski, and R. P. Van Duyne, *J. Am. Chem. Soc.*, **97**, 1699 (1975).
(58) N. Winograd and T. Kuwana, *J. Electroanal. Chem.*, **23**, 333 (1969).
(59) W. N. Hansen, *Adv. Electrochem. Electrochem. Eng.*, **9**, 1 (1973), and references therein.
(60) D. Laser and M. Ariel, *J. Electroanal. Chem.*, **35**, 405 (1972).
(61) S. Gottesfeld and M. Ariel, *J. Electroanal. Chem.*, **34**, 327 (1972).
(62) G. C. Grant and T. Kuwana, *J. Electroanal. Chem.*, **24**, 11 (1970).
(63) G. A. Gruver and T. Kuwana, *J. Electroanal. Chem.*, **36**, 85 (1972).
(64) M. Ito and T. Kuwana, *J. Electroanal. Chem.*, **32**, 415 (1971).
(65) H. N. Blount and T. Kuwana, *J. Electroanal. Chem.*, **27**, 464 (1970).

Reactions on Single-Crystal Surfaces

Gabor A. Somorjai

Materials and Molecular Research Division, Lawrence Berkeley Laboratory, and Department of Chemistry, University of California, Berkeley, California 94720

Received October 15, 1975

Reactions that require catalysis by solid surfaces have importance obvious to every chemist. They have been studied a great deal, but true understanding of just what occurs at the surface has been frustrated by difficulties in characterizing the active surfaces or in observing what happens to them as they react or catalyze a reaction.

In recent years it has been possible to obtain fundamental information about events that occur at reactive surfaces by employing techniques that are mostly new. In this work single crystals of metals are sliced so as to expose crystal faces of well-defined atomic arrangement. These faces are scrutinized by physical methods to determine surface structure and composition. A gaseous reactant can then be admitted and the kinetics of its reactions with the surface or as catalyzed by it can be studied. Finally, the very same surface can be examined during or after the reaction in order to see what changes have occurred.

The primary aim of such research is to uncover the elementary steps of surface chemical reactions. Surface reactions or catalyzed surface reactions take place under conditions of atom transport. Molecules impinge, adsorb, react on solid surfaces, and form intermediates of various lifetimes, and then the products desorb into the gas phase.

However, many of the techniques that are used to study the atomic and electronic structure of adsorbed surface species are static in nature, for example, low-energy electron diffraction (LEED) and electron or infrared spectroscopy of adsorbed molecules. Possibly static experiments that investigate the properties of adsorbates do not sense the same species that are present under conditions of atom transport. Therefore, it is of great value to combine studies of surface structure and composition with kinetic studies of reaction rate and reaction path.

In recent years there has been intensive effort in my laboratory and in others to develop techniques that permit monitoring the rates of reactions on well-characterized single-crystal surfaces of small area.[1,2] Surface reactions of low reaction probability (less than 10^{-3}) can now readily be studied on single-crystal surfaces of area approximately 1 cm^2 where the surface structure and composition is determined by LEED and Auger electron spectroscopy.

Atomic Structure of Crystal Surfaces

A solid surface is represented schematically in Figure 1. The surface is heterogeneous. There are several atomic sites that are distinguishable by the number of nearest neighbor atoms surrounding them. Atoms in terraces have the highest coordination number while adatoms, which stand singly atop a lower layer, have the lowest. Experimental evidence for the presence of these surface sites comes mostly from LEED and field ion microscopy. Atoms in terraces, in steps, and in kinks are the most numerous ($\sim 10^{14} \sim 10^{15}$ atoms/cm^2) while the concentrations of the other kinds of surface sites are orders of magnitude smaller near equilibrium.

We can vary the relative numbers of terrace, step, and kink atoms by cutting a single crystal in various directions. Figure 2 shows LEED patterns and schematic diagrams for three representative Pt surfaces that were cut in different crystallographic orientations. One of the surfaces exhibits a diffraction pattern that indicates most of the surface atoms to be in terrace positions. The second surface (Figure 2b) has steps of atomic height, 6-atom spacings apart, on the average. Stable stepped

Gabor A. Somorjai is Professor of Chemistry at University of California, Berkeley, and Principal Investigator in the Molecular Materials Research Division at Lawrence Berkeley Laboratory. He was born in Budapest, and studied at the University of Technical Sciences there for his B.S. degree. After moving to the United States, he earned the Ph.D. at Berkeley in 1960, and then joined the research staff at IBM, Yorktown Heights, N.Y. He returned to Berkeley in 1964. His principal research interests are in the field of surface science.

(1) B. Lang, R. W. Joyner, and G. A. Somorjai, *J. Catal.*, **27**, 405 (1972).
(2) G. A. Somorjai, *Catal. Rev.*, **7**, 87 (1972).